$PuPt_2In_7$: a computational and experimental investigation

H. B. Rhee,[1] F. Ronning,[2] J.-X. Zhu,[2] E. D. Bauer,[2] J. N. Mitchell,[2] P. H. Tobash,[2]
B. L. Scott,[2] J. D. Thompson,[2] Y. Jiang,[3] C. H. Booth,[3] and W. E. Pickett[1]

[1]*Department of Physics, University of California, Davis, CA 95616, USA*
[2]*Los Alamos National Laboratory, Los Alamos, New Mexico 87545, USA*
[3]*Chemical Sciences Division, Lawrence Berkeley National Laboratory, Berkeley, California 94720, USA*

(Dated: July 25, 2012)

Flux-grown single crystals of $PuPt_2In_7$ are characterized and found to be both non-superconducting and non-magnetic down to 2 K. The Sommerfeld specific heat coefficient of 250 mJ/mol K^2 indicates heavy fermion behavior. We report results of generalized gradient approximation (GGA)+U calculations of $PuPt_2In_7$ and as yet unsynthesized isovalent $PuPt_2Ga_7$. The strength of the c-f hybridization of $PuPt_2In_7$ is similar to the $PuCoIn_5$ superconductor. The bare and f-weighted susceptibility within the constant-matrix-element approximation is calculated, showing a maximum along the q_z direction at $q_x = q_y = 0.5$. A similar and slightly stronger maximum is also found in the structurally related heavy-fermion materials $PuCoGa_5$ and $PuCoIn_5$. The absence of superconductivity in $PuPt_2In_7$ is examined based on the results of our calculations.

PACS numbers: 71.20.-b, 61.05.cp, 71.27.+a

I. INTRODUCTION

Magnetically mediated superconductivity in heavy-electron systems, specifically Ce and U compounds, has been known to exist for over 30 years.[1–4] Among the known heavy fermion superconductors a particularly rich family include the so-called "115," "127," and "218" structures which are all variants of the '103' parent compound, crystallizing in the $Ho_mCo_nGa_{3m+2n}$ architecture (see Fig. 1).[5] Many of these compounds are known to be superconducting.[7–16] It is widely expected that in these systems, spin fluctuations are what bind the Cooper pairs, and the balance between these local-moment fluctuations and long-range magnetism in the vicinity of a quantum critical point is crucial for superconductivity to take place. There are however compounds that belong in this structural family but don't superconduct, as they tend to shy away from this ideal balance. For example, the f electrons in the U-115s, -218s, and the Np-115s are too itinerant to exhibit superconductivity,[17–22] and in $AmCoGa_5$ they are too localized.[23,24] $CeRhIn_5$, $CePt_2In_7$, and Ce_2RhIn_8, all nonsuperconducting antiferromagnets at ambient pressure, require compression to delocalize the f electrons and make them available for electron-electron pairing.[8,15,25] Pu-based compounds are particularly interesting, because within the actinides it is Pu that straddles the line between bearing localized and itinerant $5f$ electron states.

Pu compounds are often considered the hole analog of their Ce counterparts, for having five f electrons in the $5f_{5/2}$ spin-orbit split multiplet. In fact, the two 115 subgroups manifest very similar behaviors from their Curie–Weiss-like magnetic susceptibilities[8,13,26,27] to their quasi-two-dimensional Fermi surfaces (FSs).[28–30] The In-bearing members show remarkably similar properties as well: $PuIn_3$ is a 14 K antiferromagnet,[31] while $CeIn_3$ is a 10 K antiferromagnet,[7] and $PuCoIn_5$ and $CeCoIn_5$ are both 2 K superconductors.[9,16] Why the T_c's of the $PuCoGa_5$ and $PuRhGa_5$ superconductors are so much higher however remains elusive.

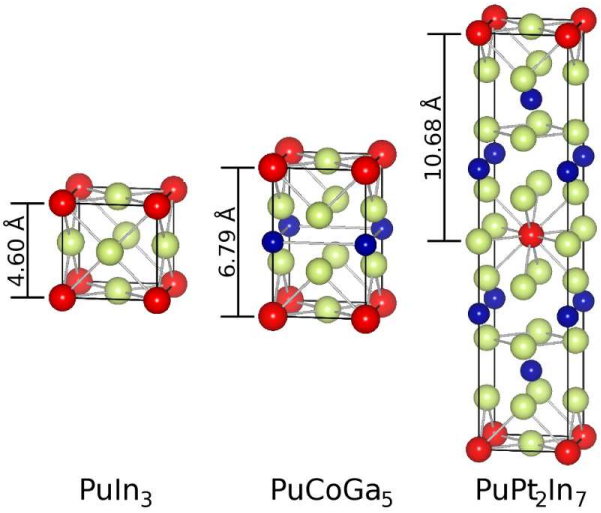

FIG. 1: (Color online.) Crystal structures, obtained using VESTA,[6] of some Pu-based compounds. The Pu atoms are colored red, Pt/Co atoms dark blue, and In/Ga atoms light green.

Based on the impressive list of superconductors discovered in the past 25 years with two-dimensional (2D) structures and properties, a guideline can be made that some aspects of 2D structures make them

TABLE I: Table of structural parameters and atomic positions for $PuPt_2In_7$ determined from single crystal X-ray diffraction.

Space group	$I4/mmm$		
a (Å)	4.5575(7)		
b (Å)	4.5575(7)		
c (Å)	21.362(6)		
Volume (Å^3)	443.71(16)		
Formula units/cell	$Z = 2$		
Atom	x	y	z
Pu	0	0	0
Pt	0	0	0.32626(6)
In1	0	0	0.5
In2	0	0.5	0.2500
In3	0	0.5	0.10597(11)

more favorable for superconductivity and will therefore give rise to a higher T_c. The average spin fluctuation frequency is higher in quasi-2D systems than 3D, and this brings about a larger Cooper pairing energy.[32] Indeed, the $PuRh_{1-x}Co_xGa_5$ ($0 \leq x \leq 1$) compounds with T_c values up to 18 K follow a linear relation in T_c vs. axial ratio c/a,[33] which is also observed in CeMIn$_5$ (and, interestingly, with an almost identical slope to its Pu-based cousins').[27,34] Recently, $CePt_2In_7$—a structurally and electronically more 2D version of 115—was discovered.[15,35] Although T_c was not enhanced, it did achieve a maximum superconducting transition temperature of 2.1 K, comparable to the other Ce-based 115s'.

In this paper, we report the discovery of the Pu analog to $CePt_2In_7$. We find $PuPt_2In_7$ is a mass enhanced paramagnet which lacks superconductivity down to 2 K. We report electronic structure calculations on $PuPt_2In_7$, including densities of states, band structures, and Fermi surfaces. We present also analogous analyses on isovalent $PuPt_2Ga_7$, which has yet to be synthesized. In addition, we have calculated the constant-matrix-element and atomic-character-matrix-element non-interacting magnetic susceptibilities of $PuPt_2In_7$ and $PuPt_2Ga_7$, and of $PuCoGa_5$ and $PuCoIn_5$ as points of comparison. While the Fermi surfaces of the 127 compounds are qualitatively distinct from the 115s, all four Pu compounds exhibit a row of peaks in the susceptibility along the q_z direction at $q_x = q_y = 0.5$. We discuss the possible implication of these results for understanding Pu-based superconductivity.

II. EXPERIMENT

Single crystals of $PuPt_2In_7$ were grown by the self flux method from the respective elements with an excess of In metal. The reactions were loaded in the ratio Pu:Pt:In (1:4:30) using 2 cm^3 alumina crucibles which were sealed under vacuum in quartz ampoules. The isolated single crystals grew with a plate-like habit and were found to be $PuPt_2In_7$ based on single crystal X-ray diffraction analysis. The single crystal X-ray data was collected on a Bruker D8 equipped with a APEX2 CCD detector. Full spheres of data were collected at room temperature and the collections were handled in batch runs at different ω and ϕ angles. The structure was refined using the atomic coordinates from the isostructural $CePt_2In_7$ compound. The data integration and refinement procedures were completed using SAINT-Plus, SHELXS97, and SHELXL97 programs. $PuPt_2In_7$ stabilizes into a body-centered tetragonal structure (see Fig. 1, Table I). While in $PuCoGa_5$ the $PuGa_3$ layer and $CoGa_2$ layer stack alternately, resulting in a primitive structure, $PuPt_2In_7$ has two layers of $PtIn_2$ for each $PuIn_3$.

To understand the local structure of $PuPt_2In_7$, fluorescence x-ray absorption fine structure (XAFS) data were collected at the Stanford Synchrotron Radiation Lightsource (SSRL) on the Pu and Pt $L_{\rm III}$-edges at beamline 11-2, using a half-tuned double crystal Si(220) monochromator, with a slit height of 0.6 mm and 0.5 mm for the measurement of each edge, respectively. A six-month old crystal sample was triply contained in a sample holder with Kapton mylar, and was 45° to the incident X-ray beam. 3 scans were collected for each edge at T = 30, 100, 200 and 300 K with a temperature deviation of less than 0.2 K. The self-absorption corrected XAFS data are reduced using standard procedures outlined in Refs. 36 and 37, including fitting an embedded-atom absorption function $\mu_0(E)$ using a 7-knot cubic spline function with a maximum photoelectron wave vector k of 15 Å^{-1}. The XAFS function is then defined as $\mu(k)/\mu_0(k) - 1$, where μ is the absorption coefficient, $k = \sqrt{(2m_e/\hbar^2)(E - E_0)}$ is the photoelectron wave vector, m_e is the electron rest mass, E is the incident energy, and E_0 is the absorption edge threshold energy, which is defined arbitrarily to be the half height of the edge and allowed to vary in the fit.

k^3-weighted EXAFS data, $k^3\chi(k)$, are fast Fourier transformed (FFT) to r space (FFT($k^3\chi(k)$)), with the FFT range of k = 3.5–13.5 Å^{-1} and Gaussian window of 0.3 Å^{-1}, for both Pu and Pt edges. The r-space EXAFS data are then fit with theoretical *FEFF* functions calculated based on the $I4/mmm$ lattice structure. The r-space data versus fit are

TABLE II: EXAFS fit results for the Pu and Pt $L_{\rm III}$-edges on $PuPt_2In_7$. Fit and Fourier transformed ranges are listed in the caption of Fig. 2. Though we only show single-scattering peaks shorter than 5.0 Å, all single- and multiple-scattering peaks within the fit range are included. To obtain a better estimate of the contribution from the farther atoms in the fit range, the single-scattering peaks between 5.4 and 6.0 Å are also included in the fit and are held together with one single σ^2. Coordination numbers N are held fixed to the nominal structure. A small vibration of the lattice is allowed by constraining the shifts of all longer bonds to the shortest bonds and keep the shortest ones free to move. In addition, in the Pt edge fit, the Pt-Pu pairs at ∼4.92 Å are fixed to the Pu-Pt pairs with the same R, and σ^2 to reduce the fitting parameter. S_0^2, ΔE, and the fit quality are 0.90(1), −10.0(1) eV, and 7.6% for the Pu edge, respectively, and 0.90(1), −8.1(15) eV, and 18.20% for the Pt edge. (Note that the bad fit quality for the Pt edge fit and large uncertainty in the correlated Debye fit for the Pt-In(1) pair are caused by the background oscillation around 3.5 Å.) The number of free parameters in the fits are 14 for the Pu and 15 for the Pt edge, far below the number of independent data points as given by Stern's rule,[40] which is ∼23 for both fits. The fraction (%) of ion/ion site interchange are shown in units of percentage.

	N	σ^2 (Å^2)	R (Å)	$\sigma^2_{\rm stat}$ (Å^2)	$\theta_{\rm cD}$ (T)
Pu-In(3)/In(1)	12	0.002(3)	3.224(4)	0.0001(1)	211(2)
Pu-Pu	4	0.004(2)	4.567	0.0015(5)	145(9)
Pu-Pt	8	0.005(3)	4.925	0.0039(4)	238(15)
Pt-In(3)/In(2)	8	0.0003(2)	2.745(6)	-0.0003(5)	266(29)
Pt-In(1)	1	0.0003	3.702	0.0009(18)	408(368)
Pt-Pt	8	0.0006(5)	4.561	-0.0001(8)	255(33)
site-interchange	Pu/In(1)	Pu/In(2)	Pu/In(3)	Pu/Pt	Pt/In(1)
fraction (%)	6±4	15±6	0±4	3±5	18±21

shown in Fig. 2; the Debye-Waller factors, $\sigma^2(T)$, for some atom pairs (< 5 Å) are fit to the correlated Debye model[38] to obtain the static distortion, $\sigma^2_{\rm stat}$, and the correlated Debye temperature, $\theta_{\rm cD}$ (shown in Table II). The Pu occupancy (∼98±16%) is estimated by allowing the amplitude of the Pu-Pu peak (4.56 Å) to vary in the Pu edge fit, though the fit quality doesn't change from the previous fit, which assumes 100% Pu occupancy. By arbitrarily constraining $\sigma^2_{\rm stat} \geq 0$ for the Pu-Pu pair, the Pu occupancy is estimated to be > 83%. Possible ion/ion site interchange, such as Pu to In(1,2,3), and Pt to In(1), are also examined using a similar method as in Ref. 39. From these fits, the percentage of Pu site-interchange with other ions, shown in lower part of Table II, is estimated to be close to zero within a small error. Hence, the fit results indicate well ordered local lattice structure around both Pu and Pt ions.

Specific heat data is shown in Fig. 3. A fit of the data to $C/T = \gamma + \beta T^2$ between 7 and 13 K gives an enhanced Sommerfeld coefficient of 250 mJ/mol K^2 and β = 3.67 mJ/mol K^4. Using the formula $\Theta_D = (12/5 * \pi^4 n k_B)^{1/3}\beta$—where k_B is the Boltzmann constant and n, the number of atoms per formula unit, is equal to 10—we get a Debye temperature, Θ_D = 174 K. The Sommerfeld coefficient is larger than that of $PuCoGa_5$ ($\gamma \simeq 100$ mJ/mol K^2). Thus, the value of γ for $PuPt_2In_7$ likely represents a reduction in the characteristic spin fluctuation temperature of $PuPt_2In_7$ relative to $PuCoGa_5$. At temperatures below 7 K, a small hump is seen in the specific heat which may represent short range correlations. Susceptibility measurements down to 2 K (not shown) have no evidence for superconductivity or long ranged magnetic order.

III. COMPUTATIONAL RESULTS

Electronic structure calculations using the generalized gradient approximation (GGA) within density functional theory[41] were carried out with WIEN2K,[42] which employs full-potential linearized augmented planewaves and local orbitals. In principle, GGA is more appropriate than LDA, as exemplified by the GGA studies by Robert, Pasturel, and Siberchicot of Pu compounds.[43] We adopted the Perdew-Burke-Ernzerhof[44] exchange-correlation potential based on the generalized gradient approximation, and we included spin-orbit (SO) interactions through a second variational method. We performed calculations with and without the Hubbard U (using the around mean field double-counting correction[45]) and exchange J; we used the widely accepted values of U = 3–4 eV, J = 0.6 eV for Pu.[20,46–49]

The experimental lattice parameters of $PuPt_2In_7$ (see Table I) were used. They were also used to estimate the size of the hypothetical compound $PuPt_2Ga_7$, by means of extrapolating the lattice

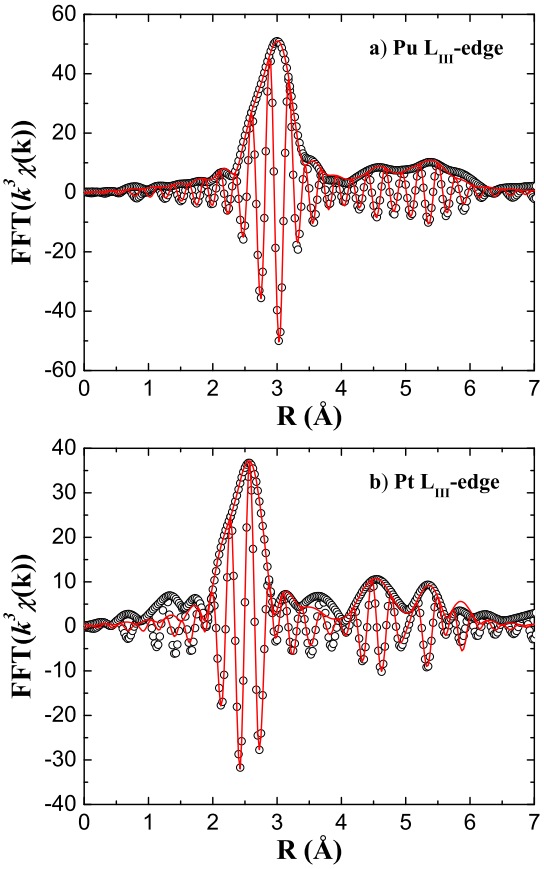

FIG. 2: Fast Fourier transformed r-space data (open symbol) and the fit (solid line) for a) Pu $L_{\rm III}$-edge and b) Pt $L_{\rm III}$-edge. Both EXAFS data were measured at $T = 30$ K, with the Fourier transformed k range of 3.5–13.5 Å^{-1} and the Gaussian window of 0.3 Å^{-1}. The r-space fit range is 2.1–5.4 Å for both edges. Here only the real part, Re, and the amplitude, $\sqrt{\mathrm{Re}^2 + \mathrm{Im}^2}$, of FFT($k^3\chi(k)$) are plotted.

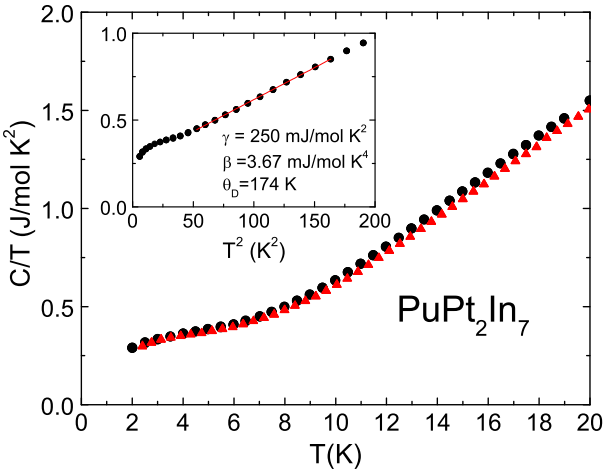

FIG. 3: (Color online) Specific heat data (C/T) vs. temperature of $PuPt_2In_7$, taken in zero field (black circles) and 6 T (red triangles). Inset shows the data plotted vs. T^2 along with a linear fit between 7 and 13 K, from which estimates of the Sommerfeld coefficient and Debye temperature were obtained.

differences of $PuCoGa_5$ (Ref. 11) and $PuCoIn_5$ (Ref. 16). The inferred lattice parameters for $PuPt_2Ga_7$ are thus $a = 4.22$ Å and $c = 19.51$ Å. The same internal parameters for $PuPt_2In_7$ were used for $PuPt_2Ga_7$.

Paramagnetic (PM), ferromagnetic (FM), and two different antiferromagnetic (AFM) calculations were performed for both $PuPt_2In_7$ and $PuPt_2Ga_7$, and the relative energies are listed in Table III. AFM I represents a configuration in which the antiferromagnetic **q**-vector is $(1/2, 1/2, 0)$, and AFM II has a wavevector of $(0, 0, 1)$. Regardless of the value of U, the energy of PM $PuPt_2In_7$ stays far above those of the other magnetic configurations—a contrast to experimental observations (although, the difference shrinks with increasing U). Even though the AMF double-counting method was implemented specifically for its suppression of magnetism,[50] and has correctly predicted the nonmagnetic ground state for δ-Pu, $PuCoGa_5$, and the Pu-218s[20,28,51] when no other double-counting approach has been successful, it fails to have the same effect on $PuPt_2In_7$. A reason for this may be that the distance between the Pu atom and its nearest neighbor is greater in $PuPt_2In_7$ (3.2 Å) than the other compounds (it is 3.0 Å for $PuCoGa_5$, 2.5 Å for Pu_2CoGa_8, and 2.6 Å for Pu_2RhGa_8; δ-Pu does not have a ligand but the Pu-Pu distance is 3.1Å), which would provide more room for larger local moments. In the GGA scheme, the ground-state configuration of $PuPt_2In_7$ is AFM I, but the FM and AFM II systems become more stable when U is set to 3 eV. At 4 eV, the AFM II configuration has the lowest energy, with the FM state just 2 meV higher. This indicates that increasing U favors FM interactions within planes and weak AFM interactions between planes.

$PuPt_2Ga_7$'s energies at $U = 0$ are not unlike $PuPt_2In_7$'s, but when U is turned on, competition for the ground state is not between FM and AFM II but the two antiferromagnetic flavors. The general similarities suggest it is likely that $PuPt_2Ga_7$ will also be a paramagnet, but with some differences in the strength and character of short-range magnetic correlations and with weak AFM interactions between planes. Similar to calculations of δ-Pu (Ref. 52), we find a sizeable cancelation of spin and orbital moments. For instance, for the AFM II state with $U = 4$ eV we have a spin moment of 4.262 $\mu_{\rm B}$ and an orbital moment of -3.404 $\mu_{\rm B}$.

TABLE III: Relative total energies (in eV) from GGA and GGA+U calculations of different magnetic configurations of the Pu-127s. The AFM I configuration has a $\mathbf{q}$-vector of $(1/2, 1/2, 0)$, AFM II has one of $(0, 0, 1)$. $J = 0.6$ eV for all $U \neq 0$ calculations.

		PM	FM	AFM I	AFM II
$PuPt_2In_7$	$U = 0$ eV	+1.15	+0.09	0.00	+0.09
	$U = 3$ eV	+0.57	0.00	+0.01	0.00
	$U = 4$ eV	+0.17	+0.002	+0.04	0.00
$PuPt_2Ga_7$	$U = 0$ eV	+0.93	+0.10	0.00	+0.11
	$U = 3$ eV	+0.41	+0.03	0.00	+0.001
	$U = 4$ eV	+0.06	+0.06	+0.01	0.00

IV. ELECTRONIC STRUCTURE

Fig. 4 shows the calculated density of states (DOS) of paramagnetic $PuPt_2In_7$ from a GGA calculation without the Coulomb U, and that from a GGA+U calculation ($U = 3$ eV and $J = 0.6$ eV are used for any GGA+U calculation mentioned henceforth). In both pictures, the Pt manifold, predominantly $5d$ in character in the region shown, ends near the -2 eV mark and is fully occupied; such is the general case for $4d$ and $5d$ metals in the 115s and 218s. Thus Pt is neutral or possibly slightly negatively charged in these compounds. In the GGA case, the two large Pu peaks correspond to the $5f_{5/2}$, $5f_{7/2}$ SO splitting of very narrow f bands. The peaks are separated by roughly 1 eV, which is the expected splitting level for Pu compounds.

With the addition of U, the Pu peaks each split into multiple smaller peaks. The occupied peak broadens to span a range of 1.5 eV; the unoccupied peak shifts 0.8 eV to the right and creates a trail of f character up to above 4 eV. The Pu bands widen as a result of the on-site Coulomb repulsion and exchange interaction J. The DOS at ε_F is $N(0) = 6.32$ eV^{-1} (down from the GGA DOS of 9.07 eV^{-1}), which gives a noninteracting electronic specific heat coefficient of 15 mJ/mol-K^2. Comparison with the experimentally measured Sommerfeld coefficient of 250 mJ/mol K^2 gives a mass renormalization of $\sim$17, which cannot be captured by our static mean-field calculations. Dynamical correlations as in the Kondo effect are responsible for this discrepancy, as observed for the other Pu compounds in this family.

Fig. 5 provides the DOS of nonmagnetic $PuPt_2Ga_7$ from GGA and GGA+U calculations. As in $PuPt_2In_7$, the Pt $5d$ states are filled and the Pu $5f$ peaks, which are located between -1 and $+1.5$ eV before the implementation of U, spread to a wider range when U is turned on. The bands are generally broader compared to $PuPt_2In_7$, due to the lattice

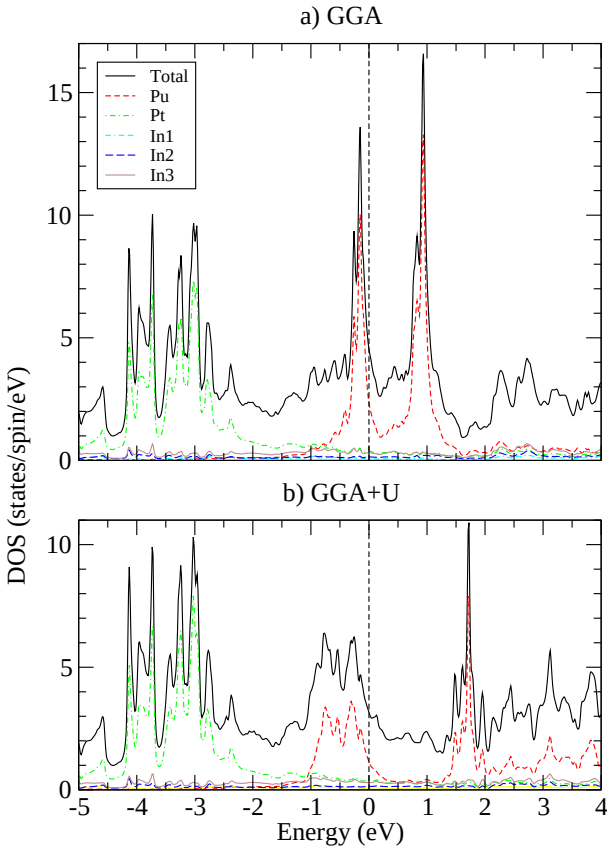

FIG. 4: (Color online) Total and partial DOSs of PM $PuPt_2In_7$ from a) GGA and b) GGA+U ($U = 3$ eV, $J = 0.6$ eV) calculations.

constants of $PuPt_2Ga_7$ (the smaller volume overrides the shortness of the Ga wavefunction). When the states near ε_F are decomposed into their total angular momentum quantum numbers m_j, we find the Pu states with $m_j = \pm 3/2$ dominate the Fermi energy. This is consistent with the idea that the most relevant hybridization will be between Pu and its nearest neighbors, which are not the in-plane but rather out-of-plane In atoms.

The band structures of PM $PuPt_2In_7$, $PuPt_2Ga_7$, and $PuCoGa_5$ obtained from GGA+U calculations are shown in Fig. 6. The thickness of a band corresponds to the weight of the f orbital. In $PuPt_2In_7$ and $PuPt_2Ga_7$, the $f_{5/2}$ and $f_{7/2}$ fatbands are visible right below and 1.5 eV above ε_F, respectively. In $PuCoGa_5$, most of the $f_{5/2}$ states are shifted downward, but the rest are concentrated at the Fermi level in relatively dispersionless form. The highly dispersive band, which spans almost 2 eV from Z to Γ and crosses the Fermi energy in $PuCoGa_5$, barely reaches ε_F in the 127s and creates a small hole Fermi surface pocket at the center of the zone

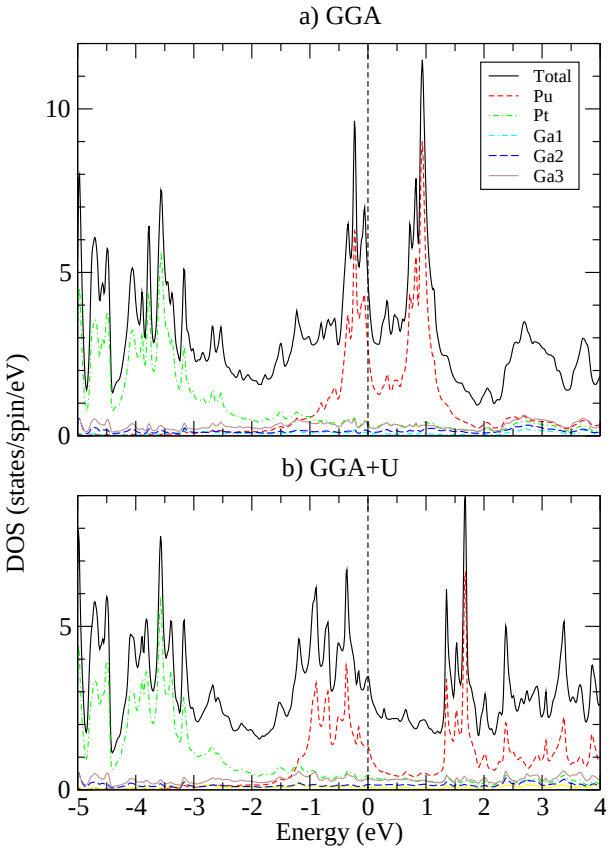

FIG. 5: (Color online) Total and partial DOSs of PM $PuPt_2Ga_7$ from a) GGA and b) GGA+U (U = 3 eV, J = 0.6 eV) calculations.

(see Fig. 7). This indicates a reduction in dimensionality when going from the 115 to the 127, but the reduction effect is not as obvious when looking at the FSs as a whole (compare Figs. 7 and 8). We therefore used WIEN2K to calculate the plasma frequency ratio $\omega_{p,xx}/\omega_{p,zz}$ $(= \langle v_x^2\rangle^{1/2}/\langle v_z^2\rangle^{1/2}$ of $PuPt_2In_7$, $PuPt_2Ga_7$, $PuCoIn_5$, and $PuCoGa_5$, and they are 2.34, 3.22, 1.46, and 1.68, respectively. As expected, all four ratios are > 1. The larger value of $PuPt_2Ga_7$ ($PuCoGa_5$) indicates two-dimensionality is enhanced when compared to $PuPt_2In_7$ ($PuCoIn_5$), despite its smaller volume. This indeed demonstrates that the 127 compounds are electronically more anisotropic than the 115 compounds. In addition, the Ga compounds, despite their smaller structure, are slightly more 2D than their In analogs.

If, as in the case of the Ce-based superconductors, the presence of superconductivity relies on the proximity to an antiferromagnetic state, we would like to know the relative degree of localization in the various Pu-115, -127, and -218 compounds. From the DFT calculations we can get an estimate for the relative strength of the c-f hybridization. We take the f-electron density within the Pu muffin-tin sphere to be inversely related to the strength of hybridization. For identically sized MT spheres (3.1) we find f-occupations of 5.24 for both $PuCoIn_5$ and $PuPt_2In_7$ and 5.14 for both $PuCoGa_5$ and $PuPt_2Ga_7$. Thus, we obtain that the In compounds are less hybridized than the Ga analogs. This result alone does not indicate the degree of localization. However, dynamical mean-field theory (DMFT) calculations show that the more weakly hybridized $PuCoIn_5$ indeed results in a smaller Kondo scale, T_0, relative to $PuCoGa_5$, and hence can be considered as more localized.[53] Thus, we can now equate the relative degree of hybridization with the relative degree of localization, and conclude that $PuCoIn_5$ and $PuPt_2In_7$ have a similar degree of localization which is stronger than the more itinerant $PuCoGa_5$ and hypothetical $PuPt_2Ga_7$. As a result, since $PuCoIn_5$ is non-magnetic it is not surprising that $PuPt_2In_7$ is also non-magnetic.

The role of the electronic structure in determining superconductivity depends on the mechanism. It has been argued that in some cases, superconductivity can be driven by Fermi surface nesting. Nesting, which indicates instability in the FS, can give rise to a spin density wave or charge density wave. In a BCS-like mechanism, even if the pairing fluctuations do not originate directly from a FS instability, the electronic structure will at a minimum determine the superconducting gap symmetry, as well as the character of the interaction. In the Pu-218s, Elgazaar *et al.* have argued that the additional FS sheets may provide sufficient differences to suppress the occurrence of superconductivity.[20] In order to see if there is any nesting present in the Pu-127s, we have used the GGA band structures to calculate the real part of the constant-matrix-element noninteracting susceptibility for $PuPt_2In_7$ and $PuPt_2Ga_7$ (see Fig. 9). In the interest of finding nesting features that are unique to the superconductors, we calculated the susceptibilities of $PuCoGa_5$ and $PuCoIn_5$ as well. The generalized susceptibility is

$$\chi(\mathbf{q}) = -\sum_{\alpha\beta\mathbf{k}} \frac{f(\varepsilon_{\alpha,\mathbf{k}}) - f(\varepsilon_{\beta,\mathbf{k+q}})}{\varepsilon_{\alpha,\mathbf{k}} - \varepsilon_{\beta,\mathbf{k+q}} + i\delta},$$

where f denotes the Fermi distribution function, $\varepsilon_{\alpha,\mathbf{k}}$ is the energy dispersion, and α and β are band indices. Alongside the conventional $\chi(\mathbf{q})$, we also calculated the susceptibility incorporating the relative weight of the Pu f orbital, so as to pick out the attributes dominated by Pu f character. In the style of Mazin as in Ref. 54, the *weighted* suscepti-

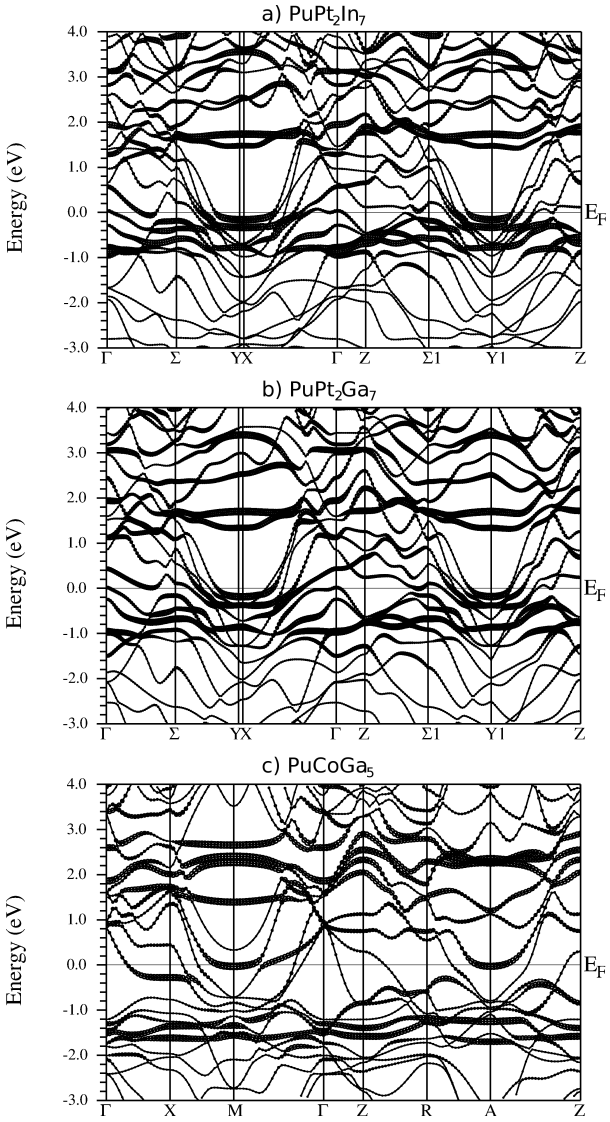

FIG. 6: GGA+U band structures of PM a) $PuPt_2In_7$, b) $PuPt_2Ga_7$, and c) $PuCoGa_5$, with f-weight fatbands.

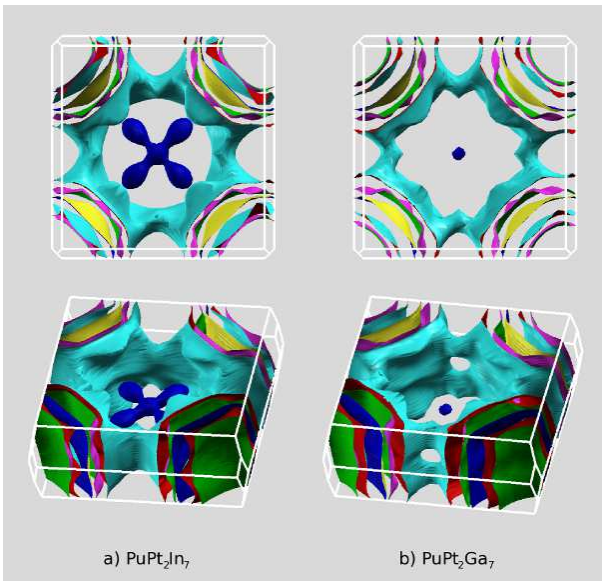

FIG. 7: (Color online) Calculated FSs of a) $PuPt_2In_7$ and b) $PuPt_2Ga_7$ in the GGA+U scheme. Γ is located in the center of the unit cell. For clarity, the 3D FSs are reproduced in the bottom figures.

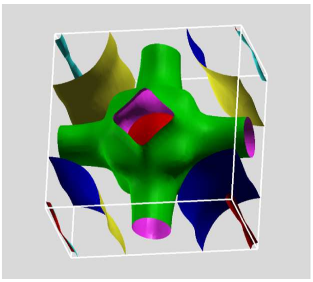

FIG. 8: (Color online) Calculated FSs of $PuCoGa_5$ in the GGA+U scheme. Γ is located in the center of the unit cell.

bility $\tilde{\chi}(\mathbf{q})$ is

$$\tilde{\chi}(\mathbf{q}) = -\sum_{\alpha\beta\mathbf{k}} \frac{f(\varepsilon_{\alpha,\mathbf{k}}) - f(\varepsilon_{\beta,\mathbf{k+q}})}{\varepsilon_{\alpha,\mathbf{k}} - \varepsilon_{\beta,\mathbf{k+q}} + i\delta} W_{\alpha,\mathbf{k}} W_{\beta,\mathbf{k+q}},$$

where W is the weight of the f orbital. Shown in Fig. 9 are the f-weighted $\tilde{\chi}(\mathbf{q})$, which are normalized and plotted along the q_xq_y plane for $q_z = 0.5$, of the four compounds. In each case, the non-weighted $\chi(\mathbf{q})$ looks almost identical to its weighted counterpart, demonstrating that the weights of other atoms and orbitals were negligible to begin with. $PuPt_2In_7$ and $PuPt_2Ga_7$ have similar-looking susceptibility plots, as do $PuCoGa_5$ and $PuCoIn_5$. Moreover, the susceptibilities of the 115s aren't very dissimilar to those of the 127s. The primary difference is that the 127s feature elevated values along $(0.5, q_x)$ (and equivalently, $(q_y, 0.5)$), which can also be seen, to a much lesser degree, in $PuCoIn_5$. The peak-like character is most pronounced for $PuCoGa_5$, which has the highest T_c of the four compounds.

Wang et al.[55] noted two peaks in $PuCoGa_5$'s $\chi(\mathbf{q})$, at $\mathbf{q} = (0.5, 0.5, 0)$ and $\mathbf{q} = (0.5, 0.5, 0.5)$. More accurately, the two peaks are part of a relatively broad ridge that, when plotted on the q_yq_z (or, equivalently, q_xq_z) plane, spans all the way in the q_z direction. This ridge is seen in all four Pu compounds, and is plotted in Fig. 10 for $PuCoGa_5$. When χ and $\tilde{\chi}$ are plotted along a q_xq_y plane for any q_z, the apex appears at the corner of the Brillouin zone

($q_x = q_y = 0.5$), as can be seen in Fig. 9. That there is little variation in the landscape when varying q_z indicates a truly 2D topography in the susceptibility for both Pu-115s and Pu-127s.

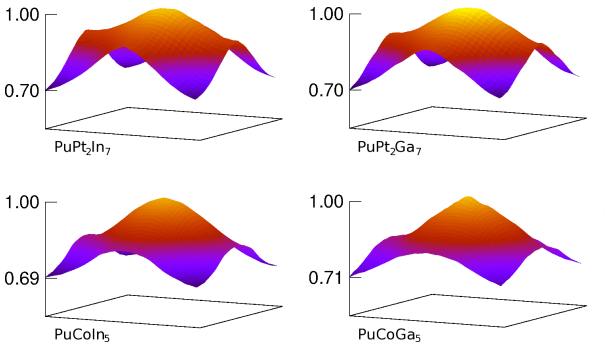

FIG. 9: (Color online) f-weighted normalized noninteracting spin susceptibilities $\tilde{\chi}$ of Pu-based compounds along the $q_x q_y$ plane in the conventional Brillouin zone for $q_z = 0.5$. $\mathbf{q} = (0, 0, 0)$ are at the corners.

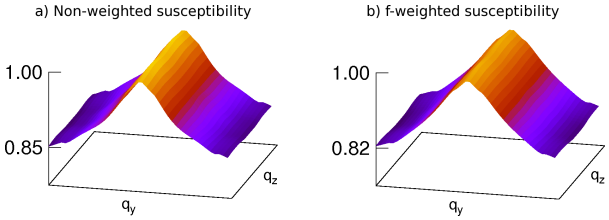

FIG. 10: (Color online) Normalized a) χ and b) $\tilde{\chi}$ of $PuCoGa_5$ in the conventional Brillouin zone for $q_x = 0.5$. $\mathbf{q} = (0, 0, 0)$ are at the corners. Susceptibilities of the other three Pu compounds look qualitatively equivalent.

When it comes to the source of the maxima $(0.5, 0.5, q_z)$, in all cases, the biggest contribution is interband nesting involving the largest FS sheet. In the 115s, the large sheet connects with the larger of the two 2D cylinders (Fig. 8); in the 127s, it maps onto the two largest cylinders (Fig. 8), where nesting with the bigger of the two cylinders is stronger than nesting with the smaller, by 7%/20% for $PuPt_2In_7$/$PuPt_2Ga_7$. Nesting between the large sheet and cylinder accounts for, on average, 32% of the susceptibility strength of $PuCoGa_5$, while that factor is only 24% for $PuCoIn_5$. Nestings between the large sheet and the two larger cylinders collectively account for 28% for $PuPt_2Ga_7$ and 26% for $PuPt_2In_7$. $PuPt_2In_7$ and $PuPt_2Ga_7$ have similar susceptibility plots, as do $PuCoGa_5$ and $PuCoIn_5$, and even the individual band-decomposed $\chi_{\alpha\beta}$'s are consistent throughout the compounds. This demonstrates the type of ligand atom has very little influence on the shape of $\chi(\mathbf{q})$.

What do these calculations tell us about superconductivity? Given the virtually identical FSs, $\chi(\mathbf{q})$, and $\tilde{\chi}(\mathbf{q})$ at the DFT level for $PuCoIn_5$ and $PuCoGa_5$ whose superconducting T_c differs by nearly an order of magnitude, suggests an additional energy scale must be important. The most likely candidate is the Kondo energy scale, T_0, extracted from either specific heat measurements or DMFT calculations. As mentioned above, earlier DMFT work on these two compounds shows that the hybridization strength inferred from DFT calculations can predict the relative trend of T_0 between various Pu-based family members.[53] Consequently, our work shows that T_0 is similar for $PuCoIn_5$ and $PuPt_2In_7$ as we as well as between $PuCoGa_5$ and $PuPt_2Ga_7$. Thus, we naively expect the scale of T_c for $PuPt_2In_7$ to be similar to $PuCoIn_5$. As a result, it is surprising that $PuPt_2In_7$ is not superconducting, especially given the similarity of the susceptibility between the Pu-115's and the Pu-127's. Of course, subtle differences do exist in $\chi(\mathbf{q})$ which may be sufficient to drive T_c below 2 K in $PuPt_2In_7$.

V. CONCLUSION

We have reported the properties of $PuPt_2In_7$ a structurally more 2D version of the known Pu-based superconductors. The gross similarities in structure and FSs between $PuPt_2In_7$ and the other known Pu-based superconductors suggest that $PuPt_2In_7$ may be a likely candidate to find superconductivity. While neither superconductivity nor magnetic order was observed down to 2 K, our calculations suggest possible ordering below 2 K. Our study of a hypothetical $PuPt_2Ga_7$ reveals strong similarites to $PuPt_2In_7$ and $PuCoGa_5$, suggesting that it is a promising candidate to find superconductivity if it can be synthesized. More work is needed to explore these various possibilities.

VI. ACKNOWLEDGMENTS

This work was supported by DOE grant DE-FG02-04ER46111, the Strategic Sciences Academic Alliance Program under grant DE-FG03-03NA00071, and by DOE SciDAC Grant No. DE-FC02-06ER25794. Work at Los Alamos was performed under the auspices of the U.S. DOE, Office of Science, Division of Materials Sciences and Engineering, and supported in part by the Laboratory Directed Research and Development program. Work at Lawrence Berkeley National Laboratory was supported by the U.S. Department of Energy (DOE),

Office of Basic Energy Sciences (BES) under Contract No. DE-AC02-05CH11231. X-ray absorption data were collected at SSRL, a national user facility operated by Stanford University on behalf of the DOE/BES.

[1] F. Steglich, J. Aarts, C. D. Bredl, W. Lieke, D. Meschede, W. Franz, and H. Schäfer, Phys. Rev. Lett. **43**, 1892 (1979).
[2] H. R. Ott, H. Rudigier, Z. Fisk, and J. L. Smith, Phys. Rev. Lett. **50**, 1595 (1983).
[3] G. R. Stewart, Z. Fisk, J. O. Willis, and J. L. Smith, Phys. Rev. Lett. **52**, 679 (1984).
[4] D. Jaccard, K. Behnia, and J. Sierro, Phys. Lett. A **163**, 475 (1992).
[5] J. D. Thompson, R. Movshovich, Z. Fisk, F.Bouquet, N. J.Curro, R. A.Fisher, P. C.Hammel, H. Hegger, M. F. Hundley, M. Jaime, P. G. Pagliuso, C. Petrovic, N. E. Phillips, and J. L.Sarrao, J. Magn. Magn. Matter **226**, 5 (2001).
[6] K. Momma and F. Izumi, J. Appl. Cryst. **41**, 653 (2008).
[7] N. D. Mathur, F. M. Grosche, S. R. Julian, I. R. Walker, D. M. Freye, R. K. W. Haselwimmer, and G. G. Lonzarich, Nature **394**, 39 (1998).
[8] H. Hegger, C. Petrovic, E. G. Moshopoulou, M. F. Hundley, J. L.Sarrao, Z. Fisk, and J. D. Thompson, Phys. Rev. Lett. **84**, 4986 (2000).
[9] C. Petrovic, P. G. Pagliuso, M. F. Hundley, R. Movshovich, J. L.Sarrao, J. D. Thompson, Z. Fisk, and P. Monthoux, J. Phys.: Condens. Matter **13**, L337 (2001).
[10] C. Petrovic, R. Movshovich, M. Jaime, P. G. Pagliuso, M. F. Hundley, J. L.Sarrao, Z. Fisk, and J. D. Thompson, Europhys. Lett. **53**, 354 (2001).
[11] J. L. Sarrao, L. A. Morales, J. D. Thompson, B. L. Scott, G. R.Stewart, F. Wastin, J. Rebizant, P. Boulet, E. Colineau, and J. H. Lander, Nature **420**, 297 (2002).
[12] G. Chen, S. Ohara, M. Hedo, Y. Uwatoko, K. Saito, M. Sorai, and I. Sakamoto, J. Phys. Soc. Jpn. **71**, 2836 (2002).
[13] F. Wastin, P. Boulet, J. Rebizant, E. Colineau, and J. H. Lander, J. Phys. Cond. Matt. **15**, S2279 (2003).
[14] D. Kaczorowski, A. P. Pikul, D. Gnida, and V. H. Tran, Phys. Rev. Lett. **103**, 027003 (2009).
[15] E. D. Bauer, H. O. Lee, V. A. Sidorov, N. Kurita, K. Gofryk, J.-X. Zhu, F. Ronning, R. Movshovich, J. D. Thompson, and T. Park, Phys. Rev. B **81**, 180507(R) (2010).
[16] E. D. Bauer, M. M. Altarawneh, P. H. Tobash, K. Gofryk, O. E. Ayala-Valenzuela, J.-N. Mitchell, R. D. McDonald, C.-H. Mielke, F. Ronning, J.-C. Griveau, E. Colineau, R. Eloirdi, R. Caciuffo, B. L. Scott, O. Janka, S. M. Kauzlarich, and J. D. Thompson, J. Phys.: Condens. Matter **24**, 052206 (2012).
[17] V. Sechovský, L. Havela, G. Schaudy, G. Hilscher, N. Pillmayr, P. Rogl, and P. Fischer, J. Magn. Magn. Mater. **104–107**, 11 (1992).
[18] K. Kaneko, N. Metoki, N. Bernhoeft, G. H. Lander, Y. Ishii, S. Ikeda, Y. Tokiwa, Y. Haga, and Y. Ōnuki, Phys. Rev. B **68**, 214419 (2003).
[19] N. Metoki, K. Kaneko, S. Raymond, J.-P. Sanchez, P. Piekarz, K. Parlinski, A. M. Oleś, S. Ikeda, T. D. Matsuda, Y. Haga, Y. Ōnuki, and G. H. Lander, Physica B **378**, 1003 (2006).
[20] S. Elgazzar, J. Rusz, P. M. Oppeneer, E. Colineau, J.-C. Griveau, N. Magnani, J. Rebizant, and R. Caciuffo, Phys. Rev. B **81**, 235117 (2010).
[21] D. Aoki, Y. Homma, Y. Shiokawa, E. Yamamoto, A. Nakamura, Y. Haga, R. Settai, and Y. Ōnuki, J. Phys. Soc. Jpn. **73**, 2608 (2004).
[22] D. Aoki, Y. Homma, Y. Shiokawa, H. Sakai, E. Yamamoto, A. Nakamura, Y. Haga, R. Settai, and Y. Ōnuki, J. Phys. Soc. Jpn. **74**, 2323 (2005).
[23] I. Opahle, S. Elgazzar, K. Koepernik, and P. M. Oppeneer, Phys. Rev. B **70**, 104504 (2004).
[24] P. Javorský, F. Jutier, P. Boulet, F. Wastin, E. Colineau, and J. Rebizant, Physica B **378**, 1007 (2006).
[25] M. Nicklas, V. A. Sidorov, H. A. Borges, P. G. Pagliuso, C. Petrovic, Z. Fisk, J. L. Sarrao, and J.-D. Thompson, Phys. Rev. B. **67**, 020506(R) (2003).
[26] N. J. Curro, B. Simovic, P. C. Hammel, P. G. Pagliuso, J. L. Sarrao, J. D. Thompson, and G. B. Martins, Phys. Rev. B **64**, 180514(R) (2001).
[27] P. G. Pagliuso, C. Petrovic, R. Movshovich, D. Hall, M. F. Hundley, J. L. Sarrao, J.-D. Thompson, and Z. Fisk, Phys. Rev. B. **64**, 100503(R) (2001).
[28] P. M. Oppeneer, A. B. Shick, J. Rusz, S. Lebégue, and O. Eriksson, J. Alloys Compd. **444**, 109 (2007).
[29] D. Hall, E. C. Palm, T. P. Murphy, S. W. Tozer, C. Petrovic, E. Miller-Ricci, L. Peabody, C. Q. H. Li, U. Alver, R. G. Goodrich, J. L. Sarrao, P. G. Pagliuso, J. M. Wills, and Z. Fisk, Phys. Rev. B **64**, 064506 (2001).
[30] R. Settai, H. Shishido, S. Ikeda, Y. Murakawa, M. Nakashima, D. Aoki, Y. Haga, H. Harima, and Y. Ōnuki, J. Phys. Cond. Matt. **13**, L627 (2001).
[31] H. Yasuoka et al., unpublished.
[32] P. Monthoux and G. G. Lonzarich, Phys. Rev. B **59**, 14598 (1999).
[33] E. D. Bauer, J. D. Thompson, J. L. Sarrao, L. A. Morales, F. Wastin, J. Rebizant, J.-C. Griveau, P. Javorsky, P. Boulet, E. Colineau, G. H. Lander, and G. R.Stewart, Phys. Rev. Lett. **93**, 147005 (2004).
[34] R. S. Kumar, H. Kohlmann, B. E. Light, A. L. Cornelius, V. Raghavan, T.-W. Darling, and J. L. Sarrao, Phys. Rev. B. **69**, 014515 (2004).
[35] M. M. Altarawneh, N. Harrison, R. D. McDonald, F. F. Balakirev, C. H. Mielke, P. H. Tobash, J.-X. Zhu, J. D. Thompson, F. Ronning, and E. D. Bauer, Phys. Rev. B **83**, 081103(R) (2011).
[36] T. M. Hayes and J. B. Boyce, Solid State Phys. **37**, 173 (1982).

[37] G. G. Li, F. Bridges, and C. H. Booth, Phys. Rev. B **52**, 6332 (1995).
[38] E. Crozier, J. Rehr, and R. Ingalls, *X-Ray Absorption: Principles, Applications, Techniques of EXAFS, SEXAFS and XANES* (Wiley, 1988), chap. 9.
[39] E. D. Bauer, C. H. Booth, G. H. Kwei, R. Chau, and M. B. Maple, Phys. Rev. B **65**, 245114 (2002).
[40] E. A. Stern, Phys. Rev. B **48**, 9825 (1993).
[41] P. Hohenberg and W. Kohn, Phys. Rev. **136**, B864 (1964).
[42] K. Schwarz and P. Blaha, Comp. Mat. Sci. **28**, 259 (2003).
[43] G. Robert, A. Pasturel, and B. Siberchicot, Phys. Rev. B **68**, 075109 (2003).
[44] J. P. Perdew, K. Burke, and M. Ernzerhof, Phys. Rev. Lett. **77**, 3865 (1996).
[45] M. T. Czyżyk and G. A. Sawatzky, Phys. Rev. B **49**, 14211 (1994).
[46] S. Y. Savrasov and G. Kotliar, Phys. Rev. Lett. **84**, 3670 (2000).
[47] A. B. Shick, V. Janiš, and P. M. Oppeneer, Phys. Rev. Lett. **94**, 016401 (2005).
[48] L. V. Pourovskii, M. I. Katsnelson, and A. I. Lichtenstein, Phys. Rev. B **73**, 060506(R) (2006).
[49] M.-T. Suzuki and P. M. Oppeneer, Phys. Rev. B **80**, 161103(R) (2009).
[50] E. R. Ylvisaker, W. E. Pickett, and K. Koepernik, Phys. Rev. B **79**, 035103 (2009).
[51] A. B. Shick, V. Drchal, and L. Havel, Europhys. Lett. **69**, 588 (2005).
[52] P. Söderlind, A. Landa, and B. Sadigh, Phys. Rev. B **66**, 205109 (2002).
[53] J.-X. Zhu, P. H. Tobash, E. D. Bauer, F. Ronning, B. L. Scott, K. Haule, G. Kotliar, R. C. Albers, and J. M. Wills, Europhys. Lett. **97**, 57001 (2012).
[54] I. I. Mazin, Phys. Rev. B **81**, 020507 (2010).
[55] J. L. Wang Z. Zeng, and H. Q. Lin, J. Appl. Phys. **99**, 08M505 (2006).